Hindawi
Journal of Nanomaterials
Volume 2019, Article ID 5924672, 8 pages
https://doi.org/10.1155/2019/5924672

Research Article

Fabrication of Ni-Doped $PbTiO_3$-Coated TiO_2 Nanorod Arrays for Improved Photoelectrochemical Performance

Yu Fu,[1] Zhi-Peng Mao,[1] Di Zhou,[1,2] Zheng-Long Hu,[3] Ya-Fang Tu,[1] Yu Tian,[1] and Guang Zheng[1]

[1]*School of Physics and Information Engineering, Jianghan University, Wuhan 430056, China*
[2]*Key Laboratory of Optoelectronic Chemical Materials and Devices of Ministry of Education, Jianghan University, Wuhan 430056, China*
[3]*Laboratory of Low-Dimension Functional Nanostructures and Devices, Hubei University of Science and Technology, Xianning 437100, China*

Correspondence should be addressed to Di Zhou; dizhou@jhun.edu.cn and Zheng-Long Hu; huzhenglong@hbust.edu.cn

Received 16 April 2019; Accepted 27 September 2019; Published 11 November 2019

Academic Editor: Alexey P. Popov

The performance of bare TiO_2 photoanodes in photoelectrochemical devices and other applications is suboptimal due to the narrow light absorption range and poor electron-hole separation. Here, heterostructured films of Ni-doped lead titanate ($PbTi_{1-x}Ni_xO_3$, PTN)-coated titania (TiO_2) nanorod arrays were fabricated via a two-step process comprising hydrothermal and sol-gel methods. In the PTN/TiO_2 composite films, the PTN component served as a visible light-responsive photosensitizer and the TiO_2 nanorod was the electron transport layer. When applied as photoanodes, the PTN/TiO_2 films achieved the maximum photoconversion efficiency of ~2.6% and a photocurrent intensity of about 4 times higher than that of the $PbTiO_3$/TiO_2 film. These results demonstrate that the ferroelectric material-coated TiO_2 heterostructured films have high potential for application in photoelectric and optical devices.

1. Introduction

The applications of photosynthetic and photocatalytic reactions based on semiconductor materials using photoelectrochemical (PEC) cells have been recognized as ideal renewable systems leveraged on green energy technology [1, 2]. Since the PEC system was first developed with TiO_2 thin film by Fujishima and Honda in 1972 [3], TiO_2 has become the most widely studied photochemical material due to its advantages of high electron mobility, high photocorrosion resistance, low cost, and nontoxicity. However, low utilization efficiency of solar energy resulting from the wide bandgap of TiO_2 (~3.0 eV for rutile and ~3.2 eV for anatase) and relatively high recombination rate of photogenerated charge carriers significantly disincentivize its application in PEC systems. To overcome these shortfalls, TiO_2 is commonly dye sensitized, ion doped, or combined with other semiconductors to form heterojunctions. As a consequence, the doping process introduces absorption states in the energy gap, enabling absorption of lower-energy photons [4–6]. Semiconductor junctions can promote separation of charge carriers through favorable energy band alignments; this potentially reduces the occurrence of recombination losses [7]. For example, many strategies have been developed to control the synthesis of heterostructured composites, such as Bi_2S_3/TiO_2 [8], Cu_2O/TiO_2 [9], and ZnO/TiO_2 [10]. In particular, TiO_2 modified by CdS quantum dots is much more exploited for PEC application and reached a maximum IPCE value of nearly 80% [11, 12]. This is aimed at improving their PEC activity by reducing the recombination rate of the photogenerated electron-hole pairs.

Since the discovery that ferroelectric oxides possess photovoltaic effect unlike the conventional semiconductors (such as CdS, Cu_2O, and Bi_2S_3) [13], ferroelectric oxides are now increasingly applied in conjunction with TiO_2. Previous studies have suggested that, in the heterostructured TiO_2

and ferroelectric oxide composites, visible light is absorbed by the ferroelectric component, in which charge carriers are generated and possibly separated by its inherent electric field, which arises from spontaneous polarization and is subsequently transferred from the ferroelectric component to TiO_2 [14–16]. In a prior work, the composite films of $BiFeO_3$ coating TiO_2 nanorod arrays were prepared to study the enhanced photocatalytic performance in visible light [17]. Lead titanate ($PbTiO_3$, PTO), a well-known solid ferroelectric oxide, exhibits excellent ferroelectric and piezoelectric properties and, thus, has been extensively investigated over the past several decades [18–20]. Since light absorption and carrier concentration both depend on bandgap, polar materials with narrow bandgap are highly desirable. Furthermore, first-principles calculations revealed that the bandgap can be reduced by doping the TiO_6 octahedron in $PbTiO_3$ with oxygen vacancy- (O vacancy-) stabilized d^8 M^{2+} ions (where M = Ni, Pd, and Pt) and, concurrently, a large polarization value is retained [21, 22].

On the other hand, for solar energy conversion based on narrow bandgap semiconductors, the controlled synthesis of vertically aligned one-dimensional (1D) nanostructures is an effective way to develop highly efficient energy conversion materials. Aligned 1D nanostructures, such as nanowires, nanotubes, and nanorods, offer a short diffusion length for holes along the radial direction, while the long axial direction of the nanostructures becomes the preferred electron channel and provides optimal length for light absorption [23, 24]. Numerous studies have reported that the aligned 1D nanostructures provide superior photocatalytic, photovoltaic, and PEC properties relative to their bulky counterparts and randomly shaped particles [25–27]. For instance, pioneer work by Lindgren et al. [28] showed the use of hematite nanorod arrays as photoanodes in a PEC cell and revealed that 1D nanostructures could potentially address some of the fundamental issues in PEC systems and improve device performance.

On the basis of the introduction above, composite heterostructured films of $PbTi_{1-x}Ni_xO_3$ (PTN, x = 0, 0.06, and 0.15, abbreviated as PTO, PTN6, and PTN15, respectively)-coated TiO_2 nanorod arrays were fabricated via a two-step process: First, the TiO_2 nanorod arrays were grown hydrothermally on F:SnO_2 (FTO) conducting substrate. This was followed by the formation of a PTN ferroelectric layer around the TiO_2 nanorods. The phase structures and morphologies of the composite films, as well as optical adsorption properties, were systematically investigated. Finally, the PEC performance was characterized under visible light irradiation.

2. Methods

2.1. Materials. All chemicals were of analytical grade and were used without further purification. Hydrochloric acid (37% mass fraction), acetic acid (CH_3COOH, 99.5%), acetylacetone ($CH_3COCH_2COCH_3$, 99.0%), tetrabutyl titanate ($Ti(OC_4H_9)_4$, 98.0%), and lead acetate ($Pb(CH_3COO)_2{\cdot}3H_2O$, 99.5%) were purchased from Sinopharm Chemical Reagent Co., Ltd., China. Nickel nitrate ($Ni(NO_3)_2{\cdot}6H_2O$, 99.99%) was purchased from Sigma-Aldrich (Shanghai) Trading Co., Ltd., China. FTO substrates were purchased from Kejing (Hefei) Materials Technology Co., Ltd., China. Deionized water was homemade at the laboratory.

2.2. Growth of TiO_2 Nanorod Arrays. TiO_2 nanorod arrays were grown on FTO conductive glass via a hydrothermal method, as previously reported [17]. Briefly, the FTO substrates were cut into rectangle pieces and ultrasonically cleaned with deionized water, acetone, and ethanol, in that order. A mixture of hydrochloric acid and deionized water (mixed at volume ratio of 1 : 1), containing a suitable amount of $Ti(OC_4H_9)_4$, was used for the hydrothermal reaction. Subsequently, the FTO was put into the autoclave containing the mixture solution and kept in an oven at 180°C for 6 h. Finally, the TiO_2 nanorod arrays were grown on the surface of the FTO substrates.

2.3. Fabrication of $Pb(Ti_{1-x}Ni_x)O_3/TiO_2$ Thin Films. Precursor solutions of PTO, PTN6, and PTN15 were prepared via a sol-gel technique. $Pb(CH_3COO)_2{\cdot}3H_2O$, $Ni(NO_3)_2{\cdot}6H_2O$, and $Ti(OC_4H_9)_4$ were used as the starting materials. Acetic acid and acetylacetone served as the solvent and chemical stabilizer, respectively. The concentration of the final solutions was adjusted to 0.3 mol/L, while the pH value was set at 3–4 with acetic acid. Subsequently, the precursor solutions were spin coated three times onto the as-prepared TiO_2 nanorod arrays to create uniform wet films. After each spin coating step, the wet films were initially dried at 180°C for 5 min to evaporate the solvent and then rapidly heated to 400°C for 10 min to remove the residual organic materials. Finally, the films were annealed at 600°C for 30 min to allow the titanate to crystallize, forming the PTN/TiO_2 composite films.

2.4. Physical Characterization. The phase structures and morphologies of the as-prepared TiO_2 nanorod arrays and PTN/TiO_2 films were characterized by X-ray diffraction (XRD, D8 Advance, with Cu $K\alpha$ radiation, Bruker Corp., Germany) and scanning electron microscopy (SEM, JSM-7100F, Hitachi Corp., Japan), respectively. The ultraviolet-visible absorption spectra were recorded with an ultraviolet-visible light (UV-Vis) spectrophotometer (UV2600, Shimadzu Corp. Japan).

2.5. PEC Measurements. The PEC performance of the TiO_2 nanorod arrays and PTN/TiO_2 composite films was measured in a three-electrode configuration on an electrochemical workstation (CHI660E, CH Instruments, Inc., Shanghai, China). The samples, a Pt foil, and Hg/HgO in aqueous KOH, served as the working, counter, and reference electrodes, respectively. A solution of 0.1 M KOH was used as the electrolyte for all of the electrochemical measurements. The effective area of the photoelectrodes was calculated to be ~0.7×0.7 cm^2 after encapsulation. The photocurrent-potential and photocurrent response curves were recorded under visible light irradiation using an AM 1.5 solar simulator with a 300 W Xe lamp (100 mW/cm^2). Electrochemical impedance spectroscopy (EIS) experiments were performed in the absence of light by applying an initial potential of

1.0 V, and the amplitude of the ac potential was kept at 5 mV over the frequency range of 0.1 Hz to 1 MHz.

3. Results and Discussion

Figure 1 shows the XRD patterns of TiO_2 nanorod arrays, PTO/TiO_2, and PTN/TiO_2 composite films. In Figure 1(a), all of the diffraction peaks, in addition to those representing the FTO substrate, can be indexed to the standard patterns of tetragonal perovskite PTO (JCPDS Card No. 70-0746) and rutile TiO_2 (JCPDS Card No. 21-1276). The XRD spectra of the composites were found to be consistent with the superposition of the two component phases, and no diffraction peak from the impurity and lead-deficient pyrochlore phases were recorded. This indicated that there was no chemical reaction between PTO and TiO_2. In Figure 1(b), it is evident that by increasing the Ni content, the (101) and (110) peaks of the PTN components become partially overlapped in the case of PTN6 and completely overlapped in the case of PTN15. The analysis reveals that the PTN6 film exhibits a multiphase coexistence of pseudotetragonal and cubic symmetries, whereas the PTN15 film contains a single phase of cubic perovskite [29, 30]. The origin of the phase transition in PTN can be attributed to the inner stress field caused by the substitution of Ti^{4+} by the larger Ni^{2+}, leading to the disruption of the Ti-O orbital hybridization balance [31].

Figure 2 displays the surface and cross-section morphologies of TiO_2 nanorod arrays and the PTO/TiO_2 and PTN/TiO_2 composite films characterized by SEM. In Figures 2(a) and 2(b), the nanorods were grown independently on the surface of FTO and were quasialigned along the plane vertical to the substrate. TiO_2 nanorods display a tetragonal cross-section with smooth side facets and rough square top facets. After being synthesized at 180°C for 6 h, the average diameter and length were estimated to be ~100 and 850 nm, respectively. Figures 2(c)–2(h) depict the surface and cross-section morphologies of the PTO/-TiO_2 and PTN/TiO_2 films. Although the nanorods cannot be identified on the surface images, PTN crystalline particles were observed. Indeed, the cross-section image shows that the voids between the nanorods were filled by the PTN components, and the thickness of the films was equivalent to the length of the nanorods. The image reveals that the pores on the surface of the films decreased gradually, indicating that the average grain size of PTN decreases with increasing Ni content. The decrease in grain size can be ascribed to the lower grain growth rate in PTN. This can be explained by Pauling's theory of electronegativity; that is, the bond energy of Ni-O is weaker than that of Ti-O because of the smaller difference in electronegativity between Ni-O (1.53) and Ti-O (1.90). This results in less heat being released during the formation of the Ni-doped PTO, leading to a slower grain growth rate and smaller grain size [32].

The optical absorption spectrum of the semiconductor is required to determine its bandgap and the corresponding photoelectrical performance. Generally, the corresponding optical bandgaps can be estimated by the tangent lines in the plot of $(\alpha h\nu)^2$ versus $h\nu$ according to Tauc's law for the direct bandgap materials, where α is the absorbance and $h\nu$ is the photon energy. However, some researchers believe that Tauc transformation should not be applied directly to the spectrum of both components together but to the spectrum of the semiconductor alone [33]. Thus, the TiO_2 nanorod arrays, PTO, and PTN thin films were prepared on FTO separately for optical absorption spectra analysis, as presented in Figure 3(a). As expected, TiO_2 nanorod arrays exhibited little absorbance at wavelengths longer than 400 nm. In contrast, the onset of the absorption occurred at a longer wavelength and exhibited a redshift when Ti in PTO was partially replaced by Ni. The absorption edge of PTN15 thin film begins at ~450 nm, which is consistent with the bandgap of 2.78 eV according to the linear fitting of the Tauc plot, as presented in Figure 3(b). These results point to the conclusion that PTN is an effective visible light-absorbing component of PTN/TiO_2 composite films.

This bandgap narrowing effect is due to the formation of new states in the electronic structure of both the highest occupied molecular orbital (HOMO) and the lowest unoccupied molecular orbital (LUMO), which are associated with the presence of Ni stabilized by an accompanying O vacancy [32]. The mechanism of bandgap narrowing due to Ni doping is shown by the inset of Figure 3(b). In PTO, the HOMO is localized around O, wherein a weak interaction occurs between the O-2*p* orbital and the Ti-3*d* and Pb-6*s* orbitals. The LUMO is localized around Ti and resembles the 3*d* state. Since the Ni and O vacancies replace those of Ti, the Ni-3*d* state falls in the bandgap of PTO, thereby reducing the bandgap of the compound. In this case, the HOMO is localized around Ni and resembles the $3d_{z^2}$ state, whereas the LUMO is localized around the Ni-3*d* state, resembling the $3d_{x^2-y^2}$ state. The tailing of the conduction band edge into the bandgap increases because the energy of the Ni-3*d* state is lower than that of the Ti-3*d* state [34]. The decrease in the bandgap improves the light absorption by the Ni-modified PTO in ultraviolet and visible regions, implying that the Ni-modified PTO can potentially increase the solar absorption efficiency of perovskite-type ferroelectrics in solar photovoltaic devices.

To assess the performance of this type of composite film in photoelectric conversion, current-voltage characteristics were investigated. The photocurrent (I) versus applied voltage (V) curves (linear voltage sweep) shown in Figure 4(a) revealed that the PTN15/TiO_2 nanorod electrode had a significantly enhanced unsaturated PEC photocurrent in the high-voltage region (above 1.5 V_{RHE}, RHE represents reversible hydrogen electrode) when compared to the other electrode materials. In the low-bias region (inset of Figure 4(a)), the PTN/TiO_2 nanorod electrodes exhibited a higher photocurrent intensity compared to the values measured under dark conditions. This indicates a higher visible light-driven PEC activity of the TiO_2 nanorod electrodes modified by the PTN photosensitizer. However, no significant difference was observed between the intensities of photocurrent and dark current of the bare TiO_2 nanorod photoanode.

To further evaluate the performance of the PTN/TiO_2 photoelectrodes, the photoconversion efficiency (η) was

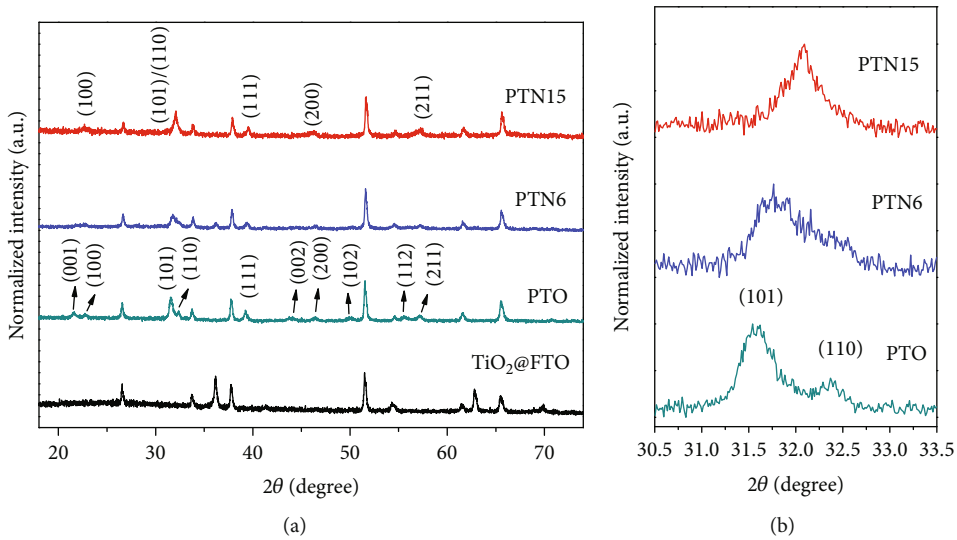

FIGURE 1: (a) XRD patterns of TiO_2, PTO/TiO_2, and PTN/TiO_2 films. (b) Enlarged XRD patterns at ~$2\theta = 32°$.

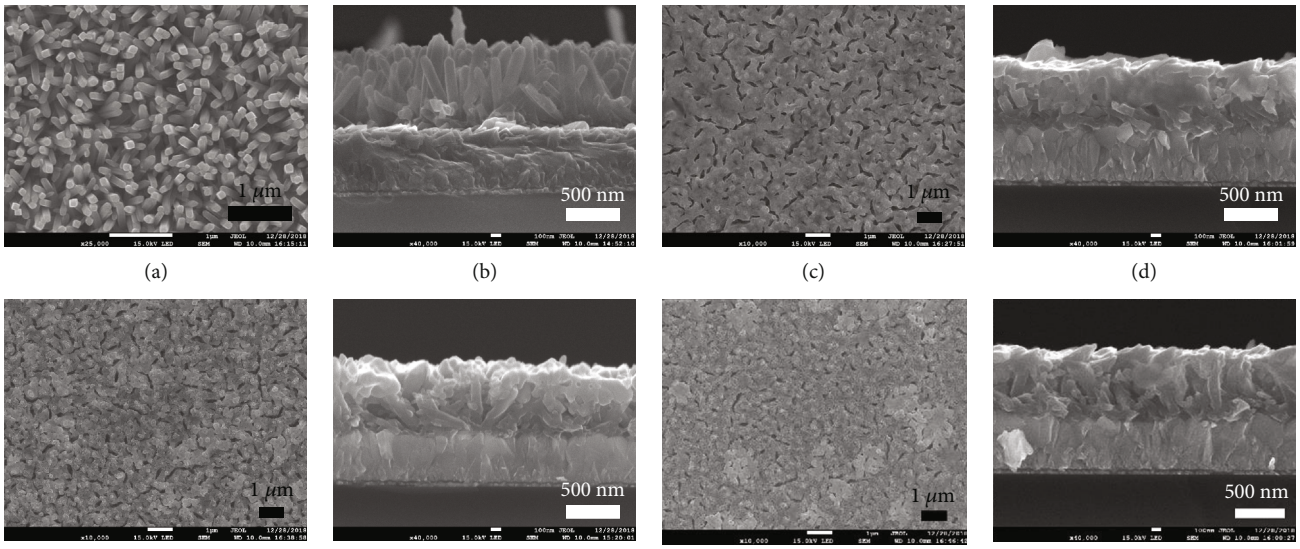

FIGURE 2: SEM images for (a) surface and (b) cross-section morphologies of TiO_2 nanorod arrays; (c) surface and (d) cross-section morphologies of PTO/TiO_2 films; (e) surface and (f) cross-section morphologies of PTN6/TiO_2 films; (g) surface and (h) cross-section morphologies of PTN15/TiO_2 films.

calculated from the photocurrent curves using the following equation [35]:

$$\eta = \frac{J(1.23 - V)}{P_{\text{light}}} \times 100\%, \quad (1)$$

where V is the applied bias versus RHE, J is the photocurrent density at the measured bias, and P_{light} is the irradiance intensity of 100 mW·cm^{-2}. Figure 4(b) shows the photocurrent efficiency versus bias potential for the PTN/TiO2 and PTO/TiO2 electrodes. The plot reveals that the PTN15/TiO2 electrode exhibits significantly higher photoconversion efficiency compared with the PTN6/TiO2 and PTO/TiO2 electrodes, and a maximum efficiency of ~2.6% was obtained at a bias potential of 2 V, which is ~10 times higher than the efficiency value of the pristine PTO/TiO2 electrode. For the PTO/TiO2 photoelectrode, the photoconversion efficiency is consistent with that reported by Chandrasekaran et al. [35] and Tabari et al. [36].

EIS is an important tool used to characterize the migration of charge carriers. The charge transport performance of the PTN-modified TiO_2 nanorod arrays is depicted in Figure 5(a), which represents Nyquist plots of PTN15/TiO_2 electrodes and the reference bare TiO_2 nanorod arrays. Generally, the arc at lower frequency of the Nyquist plot reflects

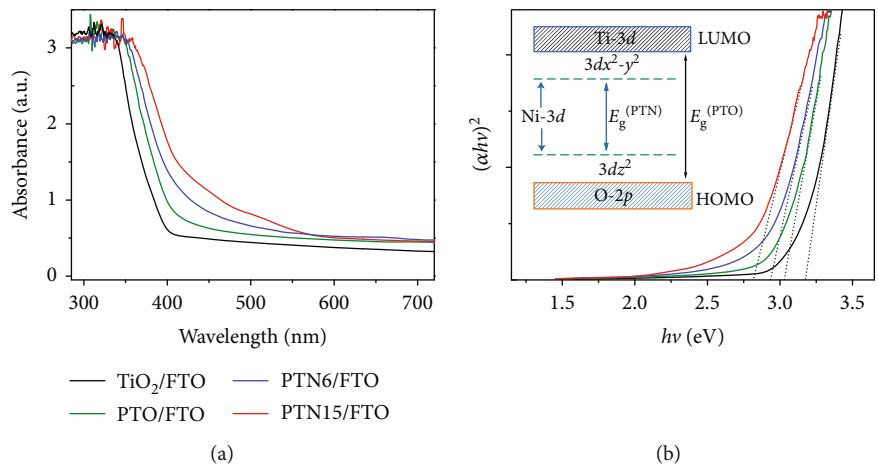

FIGURE 3: (a) UV-Vis absorption spectra of TiO_2 nanorod arrays and PTO and PTN thin films. (b) Plot of $(\alpha h\nu)^2$ versus $h\nu$ for bandgap determination. Inset: schematic illustration of the mechanism of bandgap narrowing due to Ni doping.

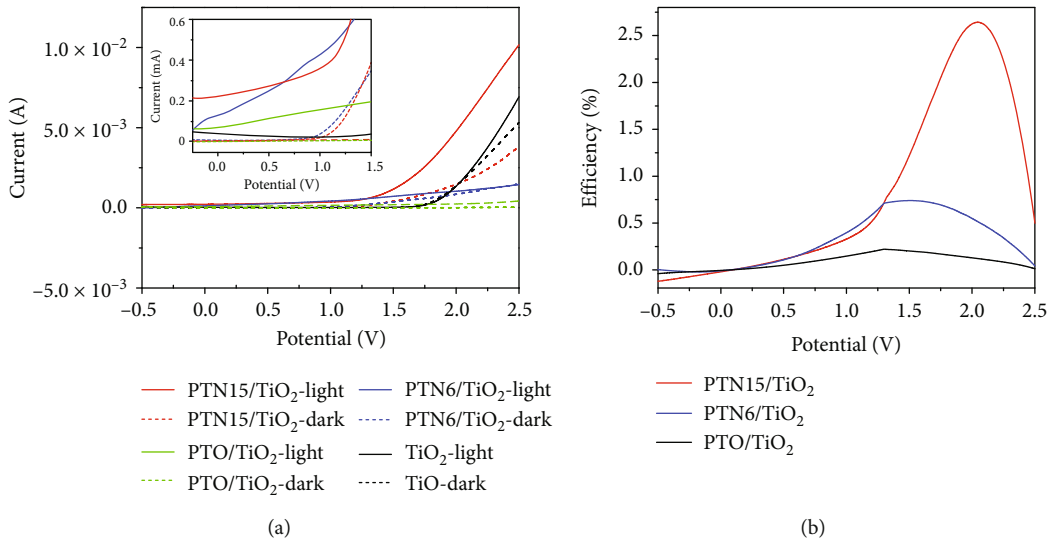

FIGURE 4: (a) I-V curves of TiO_2 nanorod arrays and the PTO/TiO_2 and PTN/TiO_2 films. Inset: magnified region of I-V curves from −0.25 to 1.5 V_{RHE}. (b) Calculated photoconversion efficiencies as a function of the applied bias for the PTO/TiO_2 and PTN/TiO_2 photoanodes.

the charge transfer impedance at the electrode/electrolyte interface, whereas a smaller arc radius stands for a faster charge transfer process with lower recombination [37]. Comparison of the EIS data revealed that PTN15/TiO_2 electrodes were considerably superior to the film of TiO_2 nanorod arrays with a smaller semicircle, demonstrating an effective charge separation and faster charge carrier transport [38, 39]. In addition, an equivalent circuit model was proposed by fitting the experimental data with analysis software (ZSimpWin, Princeton Applied Research, USA) [40], as shown in the inset of Figure 5(a). In the circuit model, R_s is the resistance of the solution, and R_1 and R_2 represent the resistance to charge transfer in the semiconductor/electrolyte and semiconductor/substrate interfaces, respectively. Q_1 and Q_2 represent the constant phase elements (CPEs) of the semiconductor/electrolyte and semiconductor/substrate interfaces, respectively [41]. The values of R_1, R_2, and R_s were calculated as 2.818×10^4, 47.15, and 0.01 $\Omega{\cdot}cm^2$ for the bare TiO_2 and 4.346×10^3, 39.9, and 0.01 $\Omega{\cdot}cm^2$ for the PTN15/TiO2 films, respectively. These results further prove that the TiO_2-PTN composite decreases the carrier transfer resistance, thereby improving the effective electron-hole separation and photoelectric conversion performance of PTN-modified TiO_2 nanorods.

Furthermore, the time-dependent photocurrent generation process (amperometric $I - t$ curves) under intermittent light irradiation is presented in Figure 5(b). The three curves reveal the rapid change in photocurrent intensity with irradiation switching, along with excellent stability and reliability during the on-off irradiation cycles. Moreover, the photocurrent intensity significantly increases with the Ni content. The photocurrent intensity of PTN15/TiO_2 films (~70 μA) is nearly 4 times higher than that of PTO/TiO_2 films (~18 μA). It is worth noting that a significant decay

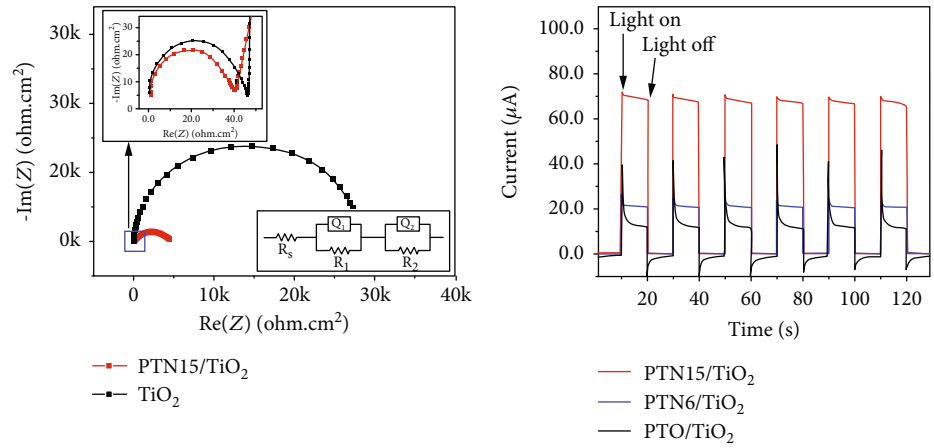

FIGURE 5: (a) Nyquist plots of EIS data for TiO_2 nanorod arrays and PTN15/TiO_2 composite films. Inset: (above) enlarged Nyquist plots at high-frequency region and (below) an equivalent circuit model of the three-electrode system. (b) Photocurrent-time transient response of the PTO/TiO_2 and PTN/TiO_2 films.

with the light on and a burst with the light off were observed in the curve of PTO/TiO_2. The main reason of photocurrent decay can be attributed to the recombination of photogenerated electron-hole [42]. The surface polarization charges formed on PTO might be a key reason for the photocurrent explosion with light off. In contrary, the recombination of photogenerated electron-hole on the surface of PTN/TiO_2 is reduced with the doping of Ni. Meanwhile, ferroelectric polarization is also reduced in PTN with the introduction of Ni, which leads to the burst of photocurrent that was not observed.

4. Conclusions

In conclusion, Ni-doped PTO ferroelectric material-coated TiO_2 nanorod films were fabricated by growing TiO_2 nanorod arrays via a hydrothermal method and synthesizing ferroelectric PTN by a sol-gel method. After annealing, the PTO ferroelectric crystals partially substituted with Ni in B-sites were deposited on TiO_2 nanorods as optical absorbers. The integration of TiO_2 nanorods and PTN ferroelectric material dramatically extended the wavelength range for light absorption and reduced the charge transfer resistance. This, in turn, facilitated charge separation and electron transfer, resulting in an improved PEC activity under visible irradiation when compared to the individual component phases. Herein, the PTN/TiO_2 composite displayed high potential as a photoanode agent, with high sensitivity to visible light, presenting a new approach of developing effective ferroelectric material-modified TiO_2 assemblies for photoelectronic applications and solar photovoltaic device integration.

Abbreviations

PTN: Ni-doped lead titanate, $PbTi_{1-x}Ni_xO_3$
PTN6: $PbTi_{0.94}Ni_{0.06}O_3$
PTN15: $PbTi_{0.85}Ni_{0.15}O_3$
PTN/TiO_2: $PbTi_{1-x}Ni_xO_3/TiO_2$
PTO/TiO_2: $PbTiO_3/TiO_2$
PEC: Photoelectrochemical
FTO: F-doped SnO_2
JCPDS: Joint Committee on Powder Diffraction Standards
XRD: X-ray diffraction
SEM: Scanning electron microscopy
UV-Vis: Ultraviolet-visible light
HOMO: Highest occupied molecular orbital
LUMO: Lowest unoccupied molecular orbital
EIS: Electrochemical impedance spectroscopy
O vacancy: Oxygen vacancy.

Data Availability

All data supporting the conclusions of this article are included within this article.

Conflicts of Interest

DZ is a lecturer and a Ph.D. degree holder specializing in the investigation of photoelectric and nanometer materials. GZ is a professor and a Ph.D. degree holder specializing in the investigation of functional materials. ZLH is an associate professor and a Ph.D. degree holder specializing in the investigation of optical materials. YFT and YT are associate professors and Ph.D. degree holders specializing in the investigation and characterization of electrochemistry. YF and ZPM are graduate students major in the study of nanometer materials. The authors declare that they have no competing interests.

Authors' Contributions

YF drafted the manuscript. YF and ZPM performed the experimental works. YFT, YT, and GZ carried out the series characterization of the samples and interpreted the data. DZ and ZLH conceived the idea of experiments and

amended the manuscript. All authors read and approved the final manuscript.

Acknowledgments

Authors thank LetPub (https://www.letpub.com) for its linguistic assistance during the preparation of this manuscript. This work was financially supported by the National Natural Science Foundation of China (Grant Numbers: 51502114 and 61575085).

References

[1] Z. S. Li, W. J. Luo, M. L. Zhang, J. Y. Feng, and Z. G. Zou, "Photoelectrochemical cells for solar hydrogen production: current state of promising photoelectrodes, methods to improve their properties, and outlook," *Energy & Environmental Science*, vol. 6, no. 2, pp. 347–370, 2013.

[2] P. Lianos, "Production of electricity and hydrogen by photocatalytic degradation of organic wastes in a photoelectrochemical cell: the concept of the Photofuelcell: a review of a re-emerging research field," *Journal of Hazardous Materials*, vol. 185, no. 2-3, pp. 575–590, 2011.

[3] A. Fujishima and K. Honda, "Electrochemical photolysis of water at a semiconductor electrode," *Nature*, vol. 238, no. 5358, pp. 37-38, 1972.

[4] K. Liu, W. Zhang, F. Lei, L. Liang, and Y. Xie, "Nitrogen-doping induced oxygen divacancies in freestanding molybdenum trioxide single-layers boosting electrocatalytic hydrogen evolution," *Nano Energy*, vol. 30, pp. 810–817, 2016.

[5] S. Park, S. Kim, H. J. Kim et al., "Hierarchical assembly of TiO_2-$SrTiO_3$ heterostructures on conductive SnO_2 backbone nanobelts for enhanced photoelectrochemical and photocatalytic performance," *Journal of Hazardous Materials*, vol. 275, pp. 10–18, 2014.

[6] S. Li, Y. H. Lin, B. P. Zhang, J. F. Li, and C. W. Nan, "$BiFeO_3$/-TiO_2 core-shell structured nanocomposites as visible-active photocatalysts and their optical response mechanism," *Journal of Applied Physics*, vol. 105, no. 5, article 054310, 2009.

[7] M. A. Mohamed, J. Jaafar, M. F. M. Zain et al., "Concurrent growth, structural and photocatalytic properties of hybridized C, N co-doped TiO_2 mixed phase over g-C_3N_4 nanostructured," *Scripta Materialia*, vol. 142, pp. 143–147, 2018.

[8] S. L. Li, J. L. Huang, X. M. Ning, Y. C. Chen, and Q. K. Shi, "Preparation and photoelectrochemical performance of nano Bi_2S_3–TiO_2 composites," *Functional Materials Letters*, vol. 11, no. 3, article 1850055, 2018.

[9] V. V. Pham, D. P. Bui, H. H. Tran et al., "Photoreduction route for Cu_2O/TiO_2 nanotubes junction for enhanced photocatalytic activity," *RSC Advances*, vol. 8, no. 22, pp. 12420–12427, 2018.

[10] V. Lachom, P. Poolcharuansin, and P. Laokul, "Preparation, characterizations and photocatalytic activity of a ZnO/TiO_2 nanocomposite," *Materials Research Express*, vol. 4, no. 3, article 035006, 2017.

[11] R. D. Baker and V. P. Kamat, "Photosensitization of TiO_2 nanostructures with CdS quantum dots: particulate versus tubular support architectures," *Advanced Functional Materials*, vol. 19, no. 5, pp. 805–811, 2009.

[12] R. Zazpe, H. Sopha, J. Prikryl et al., "A 1D conical nanotubular TiO_2/CdS heterostructure with superior photon-to-electron conversion," *Nanoscale*, vol. 10, no. 35, pp. 16601–16612, 2018.

[13] T. Choi, S. Lee, Y. J. Choi, V. Kiryukhin, and S. W. Cheong, "Switchable ferroelectric diode and photovoltaic effect in $BiFeO_3$," *Science*, vol. 324, no. 5923, pp. 63–66, 2009.

[14] Y. L. Zhang, A. M. Schultz, P. A. Salvador, and G. S. Rohrer, "Spatially selective visible light photocatalytic activity of $TiO_2/BiFeO_3$ heterostructures," *Journal of Materials Chemistry*, vol. 21, no. 12, pp. 4168–4174, 2011.

[15] L. Li, X. Liu, Y. L. Zhang et al., "Visible-light photochemical activity of heterostructured core-shell materials composed of selected ternary titanates and ferrites coated by TiO_2," *ACS Applied Materials & Interfaces*, vol. 5, no. 11, pp. 5064–5071, 2013.

[16] L. Li, Y. Zhang, A. M. Schultz, X. Liu, P. A. Salvador, and G. S. Rohrer, "Visible light photochemical activity of heterostructured $PbTiO_3$_TiO_2 core–shell particles," *Catalysis Science & Technology*, vol. 2, no. 9, pp. 1945–1952, 2012.

[17] Y. Fu, Z. P. Mao, D. Zhou et al., "Preparation of $BiFeO_3$-overcoated TiO_2 nanorod arrays for the enhanced visible-light activity," *Materials Research Express*, vol. 6, article 1050c6, 2019.

[18] Z. F. Chen, Z. Wang, X. M. Li et al., "Flexible piezoelectric-induced pressure sensors for static measurements based on nanowires/graphene heterostructures," *ACS Nano*, vol. 11, no. 5, pp. 4507–4513, 2017.

[19] Q. Ji, P. Xue, H. Wu, Z. Pei, and X. Zhu, "Structural characterizations and dielectric properties of sphere- and rod-like $PbTiO_3$ powders synthesized via molten salt synthesis," *Nanoscale Research Letters*, vol. 14, no. 1, p. 62, 2019.

[20] Z. Y. Liu, Z. H. Ren, Z. Xiao et al., "Size-Controlled Single-Crystal Perovskite $PbTiO_3$ Nanofibers from Edge-Shared TiO_6 Octahedron Columns," *Small*, vol. 8, no. 19, pp. 2959–2963, 2012.

[21] J. W. Bennett, I. Grinberg, and A. M. Rappe, "New highly polar semiconductor ferroelectrics through d^8 cation-O vacancy substitution into $PbTiO_3$: a theoretical study," *Journal of the American Chemical Society*, vol. 130, no. 51, pp. 17409–17412, 2008.

[22] G. Y. Gou, J. W. Bennett, H. Takenaka, and A. M. Rappe, "Post density functional theoretical studies of highly polar semiconductive $Pb(Ti_{1-x}Ni_x)O_{3-x}$ solid solutions: effects of cation arrangement on band gap," *Physical Review B*, vol. 83, no. 20, article 205115, 2011.

[23] Q. P. Chen, J. H. Li, B. X. Zhou et al., "Preparation of well-aligned WO_3 nanoflake arrays vertically grown on tungsten substrate as photoanode for photoelectrochemical water splitting," *Electrochemistry Communications*, vol. 20, pp. 153–156, 2012.

[24] X. Y. Li, K. Peng, H. X. Chen, and Z. J. Wang, "TiO_2 nanoparticles assembled on kaolinites with different morphologies for efficient photocatalytic performance," *Scientific Reports*, vol. 8, no. 1, p. 11663, 2018.

[25] R. Kisslinger, A. M. Askar, U. K. Thakur et al., "Preferentially oriented TiO_2 nanotube arrays on non-native substrates and their improved performance as electron transporting layer in halide perovskite solar cells," *Nanotechnology*, vol. 30, article 204003, 2019.

[26] S. Hanna, K. Milos, N. Siowwoon et al., "Highly efficient photoelectrochemical and photocatalytic anodic TiO_2 nanotube layers with additional TiO_2 coating," *Applied Materials Today*, vol. 9, pp. 104–110, 2017.

[27] K. Rajeshwar, M. E. Osugi, W. Chanmanee et al., "Heterogeneous photocatalytic treatment of organic dyes in air and aqueous media," *Journal of Photochemistry and Photobiology C: Photochemistry Reviews*, vol. 9, no. 4, pp. 171–192, 2008.

[28] T. Lindgren, H. L. Wang, N. Beermann, L. Vayssieres, A. Hagfeldt, and S. E. Lindquist, "Aqueous photoelectrochemistry of hematite nanorod array," *Solar Energy Materials and Solar Cells*, vol. 71, no. 2, pp. 231–243, 2002.

[29] X. Xue, G. Tan, H. Ren, and A. Xia, "Structural, electric and multiferroic properties of Sm-doped $BiFeO_3$ thin films prepared by the sol–gelprocess," *Ceramics International*, vol. 39, no. 6, pp. 6223–6228, 2013.

[30] Y. H. He, Z. Wang, W. C. Jin et al., "Phase boundary and annealing dependent piezoelectricity in lead-free $(K,Na)NbO_3$ nanorod arrays," *Applied Physics Letters*, vol. 110, no. 21, article 212904, 2017.

[31] J. L. Zhu, H. W. Xu, J. Z. Zhang, C. Q. Jin, L. P. Wang, and Y. S. Zhao, "Thermal equations of state and phase relation of $PbTiO_3$: A high *P-T* synchrotron x-ray diffraction study," *Journal of Applied Physics*, vol. 110, no. 8, article 084103, 2011.

[32] W. L. Zhou, H. M. Deng, L. Yu, P. X. Yang, and J. H. Chu, "Magnetism switching and band-gap narrowing in Ni-doped $PbTiO_3$ thin films," *Journal of Applied Physics*, vol. 117, no. 19, article 194102, 2015.

[33] P. Makuła, M. Pacia, and W. Macyk, "How to correctly determine the band gap energy of modified semiconductor photocatalysts based on UV-vis spectra," *Journal of Physical Chemistry Letters*, vol. 9, no. 23, pp. 6814–6817, 2018.

[34] W. L. Zhou, H. M. Deng, P. X. Yang, and J. H. Chu, "Structural phase transition, narrow band gap, and room-temperature ferromagnetism in $[KNbO_3]_{1-x}[BaNi_{1/2}Nb_{1/2}O_{3-\delta}]_x$ ferroelectrics," *Applied Physics Letters*, vol. 105, no. 11, article 111904, 2014.

[35] S. Chandrasekaran, E. J. Kim, J. S. Chung et al., "Structurally tuned lead magnesium titanate perovskite as a photoelectrode material for enhanced photoelectrochemical water splitting," *Chemical Engineering Journal*, vol. 309, pp. 682–690, 2017.

[36] T. Tabari, M. Ebadi, D. Singh, B. Caglar, and M. B. Yagci, "Efficient synthesis of perovskite-type oxide photocathode by nonhydrolytic sol-gel method with an enhanced photoelectrochemical activity," *Journal of Alloys and Compounds*, vol. 750, pp. 248–257, 2018.

[37] Q. Liu, F. Wu, F. Cao et al., "A multijunction of $ZnIn_2S_4$ nanosheet/TiO_2 film/Si nanowire for significant performance enhancement of water splitting," *Nano Research*, vol. 8, no. 11, pp. 3524–3534, 2015.

[38] X. Pan, Y. Zhao, S. Liu, C. L. Korzeniewski, S. Wang, and Z. Y. Fan, "Comparing Graphene-TiO_2 Nanowire and Graphene-TiO_2 Nanoparticle composite photocatalysts," *ACS Applied Materials & Interfaces*, vol. 4, no. 8, pp. 3944–3950, 2012.

[39] N. Li, G. Liu, C. Zhen, F. Li, L. L. Zhang, and H. M. Cheng, "Battery performance and photocatalytic activity of mesoporous anatase TiO_2 Nanospheres/Graphene composites by template-free self-assembly," *Advanced Functional Materials*, vol. 21, no. 9, pp. 1717–1722, 2011.

[40] Y. Z. Chen, A. X. Li, M. Jin, L. N. Wang, and Z. H. Huang, "Inorganic nanotube/organic nanoparticle hybrids for enhanced photoelectrochemical properties," *Journal of Materials Science & Technology*, vol. 33, no. 7, pp. 728–733, 2017.

[41] R. Raza, H. Y. Qin, L. D. Fan, K. Takeda, M. Mizuhata, and B. Zhu, "Electrochemical study on co-doped ceria-carbonate composite electrolyte," *Journal of Power Sources*, vol. 201, pp. 121–127, 2012.

[42] H. Lee, H.-Y. Joo, C. Yoon et al., "Ferroelectric $BiFeO_3$/TiO_2 nanotube heterostructures for enhanced photoelectrochemical performance," *Current Applied Physics*, vol. 17, no. 5, pp. 679–683, 2017.